ERF2010_109

Dynamic Behaviour and Response of a Two–Bladed Gimballed Rotor

Giulio Avanzini*
Politecnico di Torino, Turin, 10129, Italy
Guido De Matteis†
"Sapienza" Università di Roma, Rome, 00184, Italy
Federica F. Lucertini‡
"Sapienza" Università di Roma, Rome, 00184, Italy
and
Alberto Torasso§
Politecnico di Torino, Turin, 10129, Italy

Abstract

This paper aims to analyze the characteristics of a novel, two-bladed gimbaled rotor featuring a homokinetic joint between driving shaft and rotor yoke and a fly-bar with paddles. The design and testing of this novel rotor configuration is part of the development program of a lightweight helicopter in the VLR rotorcraft certification framework. The rotor is designed with the main objective of solving some of the negative issues that affect the use of teetering rotors on light helicopters, such as strong 2/rev oscillatory loads, poor response at low g's and a pronounced sensitivity to gusts and/or large pilot inputs. A simple dynamic model is developed to allow for the interpretation of periodic motions of the system and to determine the effects of design parameters on the rotor response by means of numerical simulation and a stability analysis, a study carried out to fully assess the possible advantages of the gimbaled configuration with respect to a more traditional teetering rotor.

*Assistant Professor, Department of Aerospace Engineering, C.so Duca degli Abruzzi 24, e–mail: *giulio.avanzini@polito.it*, tel. +39 011 5646831, fax +39 011 5646899; AIAA Senior Member.

†Professor, Department of Mechanical and Aerospace Engineering, Via Eudossiana 18, e–mail: *dematteis@dma.ing.uniroma1.it*, tel. +39 06 44585210, fax +39 06 4882576; AIAA Senior Member.

‡Ph. D., Department of Mechanical and Aerospace Engineering, Via Eudossiana 18, e–mail: *federica.lucertini@uniroma1.it*.

§Ph. D. Student, Department of Aerospace Engineering, C.so Duca degli Abruzzi 24, e–mail: *alberto.torasso@polito.it*, tel. +39 011 5646871, fax +39 011 5646899; AIAA Member.

Nomenclature

a	lift curve slope of the blade/paddle section
c	blade/paddle chord
I_1,I_2	moments of inertia about feathering and flapping axes, respectively
K	hub stiffness
K_T	feathering hinge stiffness
$\bar{p}$, $\bar{q}$	roll and pitch rates of the non-rotating shaft frame in wind axes
R	blade radius
R_1,R_2	fly–bar root cut–out and radius
R_{fb}	fly–bar mean radius $= (R_2 + R_1)/2$.
u_1, u_2	hub tilt angles in the non-rotating frame
Greek symbols	
β, η	hub flapping and feathering angles
γ_{bl}	blade Lock number $= 2\rho a_{bl} c_{bl} R^4/I_2$
γ_{fb}	Lock number of fly–bar $= 2\rho a_{fb}(R_2 - R_1)c_{fb}R_{fb}^3/I_1$
θ	blade pitch angle
θ_0	collective pitch command
θ_c	cyclic pitch angle
θ_{SW}	longitudinal cyclic pitch command
λ	non–dimensional uniform inflow velocity
μ	advance ratio
ρ	air density
ϕ_{SW}	lateral cyclic pitch command
ψ	blade anomaly
Ω	rotor angular speed
Subscripts	
bl	blade
fb	fly-bar

H hub frame
R rotating–shaft frame

Introduction

In this paper the behaviour of a novel two–bladed rigid gimballed rotor equipped with fly–bar and paddles will be analyzed in order to outline possible advantages and peculiarities with respect to more conventional teetering rotors of equivalent size, for use on a light helicopter.

In spite of the extensive literature dealing with rotor dynamic behaviour, two–bladed teetering rotors received a marginal attention from the researchers. Teetering rotors were adopted in the past for relatively large military rotorcraft, such as the Bell models 205 [1] and 212. Nowadays they are still popular for light helicopters, such as the Robinson R–22, and remotely piloted vehicles (RPV) like the Yamaha R–Max, as far as the two–bladed configuration has several advantages in the framework of low–cost rotorcraft: it allows for storage in smaller hangars than those required by larger, three or four–bladed rotors, and, at the same time, the simpler configuration, featuring a single flapping hinge and no lag hinges reduces maintenance costs. Light helicopter using teetering rotors are also renowned for some disadvantages, especially in terms of vibrations transmitted to the vehicle and possible instabilities that resulted into serious accidents, such as the mast–bumping phenomenon [2].

Teetering rotor dynamic characteristics are often improved by means of additional devices, such as a stabilizing Bell bar, as on the AB–47 helicopter, or the Bell–Hiller bar, featuring aerodynamic paddles, such as in the Yamaha R–Max RPV [3]. These devices are effective in improving the dynamic characteristics of the rotor, especially during manoeuver transients, yet they are designed on the grounds of some reasonable engineering practice, previous experience and flight testing. A simple model that describes teetering rotor dynamics was derived by Chen [4] as a particular case of articulated rotor blades, but to the authors' knowledge, a systematic analysis of the effects of stabilizing bars on the dynamics of teetering rotors is not reported in the available scientific literature.

A two–bladed gimballed rotor was considered in the 60's as a possible configuration for heavy lift helicopters with tip jets and no pitch hinge [5]. The spherical hinge, allowing for feathering motion, and a blade circulation control based on small jets distributed along the blade span should have allowed for full rotor control. The model developed in [5] represents the starting point for the development of a more complete one, at the basis of the study of a two–bladed gimballed rotor configuration discussed in this paper, featuring a fly–bar with paddles, which is being considered as a possible way for alleviating some of the drawbacks that affect conventional teetering rotors.

The configuration here considered relies on a rigid yoke articulated with respect to the shaft by means of a spherical hinge, realized by means of a set of elastomeric springs to improve the handling qualities of the helicopter at low load factor. Two rigid blades are connected to the hub yoke by means of coning hinges, while the fly–bar features two low–aspect–ratio paddles at the tips. Finally the hub has some underslung to address the issue of 2/rev loads due to the hub springs. From the purely mechanical standpoint, this configuration allows one more degree of freedom to the blades in the rotating frame with respect to a conventional teetering rotor, as the flapping motion around the axis perpendicular to both the shaft and blade axes is accompanied by a feathering motion around the blade axis itself, this latter rotation corresponding to the flap angle for the fly–bar. The actual pitch angle of each blade will thus result from the combination of the direct command, delivered by a conventional swash–plate, and the feathering motion of the rotor.

The analysis of the system is carried out using a relatively simple dynamical model capable of describing the effects of various rotor-bar parameters and suitable for understanding the peculiar characteristics in terms of periodic motions and stability of this novel gimbaled rotor. The presence of a sustained wobbling motion is probably the principal characteristic of the two–bladed gimbaled rotor, as already observed in Refs. [5, 6].

As a first step, the validity of the simple model is assessed by comparison with a more accurate nonlinear model of the same rotor in order to verify the consistency of predictions at different flight speed, as long as the baseline model presents significant simplifications in the evaluation of blade and paddle aerodynamics. In spite of the availability of a more accurate model, the study is based on the simplified one, because (i) it allows to highlight in a more straightforward way the physical mechanism at the basis of the dynamic behaviour of the rotor, (ii) a more effi-

cient search in the parameter space that define the rotor configuration is possible, for identifying those values that either cause critical phenomena or provide a better response and (iii) a rigorous stability analysis is possible, based on this simple linear model.

Numerical simulations are then considered to analyze the effects of principal design parameters of the configuration such as hub spring and feathering hinge stiffness on the wobbling motion and the resulting loads transmitted to the rotor shaft. Finally, rotor stability is investigated to fully evaluate the possible advantages of the gimbaled configuration, by ruling out the insurgence of unstable motions.

In what follows, the formulation of rotor model is outlined in the next Section. The accuracy of the simplified model is assessed, the main features of the wobbling motion are discussed and the effect of design parameters on the stability of the system is analyzed. A section of conclusions ends the paper.

Rotor Model

The simplified model of the rotor sketched in Fig. 1 is developed under the following assumptions:

- rotor blades are rigid in bending and torsion
- rotor angular rate is constant
- blade cg's lies on the feathering axes
- the pitch angle of the paddles is constant
- airfoil lift coefficient is a linear functions of the angle of attack
- compressibility, unsteady aerodynamics, stall and reversed flow effects are neglected
- a uniform quasi–static inflow is assumed
- tilt angles of the hub are small
- blade twist and rotor undersling are not taken into consideration, and coning angle is zero.

With reference to [7] for the details on the formulation of the mathematical model of the rotor system, the non–dimensional equations of motion are expressed as follows, in the reference frame (x_H, y_H, z_H) of rotating, hub-fixed principal axes of inertia

$$\tilde{\omega}_1' = -\tilde{\omega}_2 + \frac{N_1}{I_1\Omega^2} \quad (1)$$

$$\tilde{\omega}_2' = \tilde{\omega}_1 + \frac{N_2}{I_2\Omega^2} \quad (2)$$

The kinematic model is written in terms of β and η that, under the small angle assumption, correspond

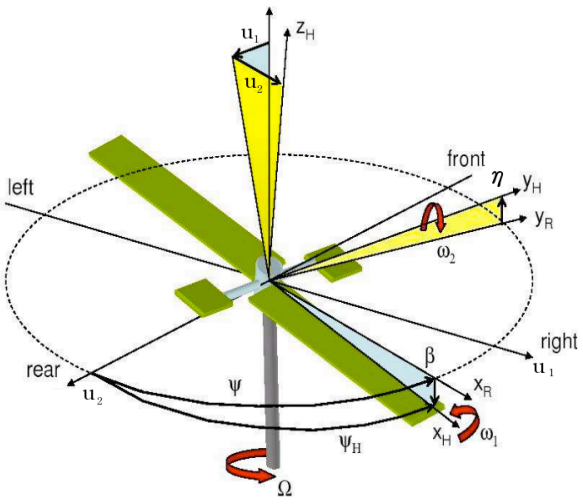

Figure 1: Rotor coordinate system.

to the flapping and feathering angles of the hub with respect to the rotating shaft–fixed frame (x_R, y_R, z_R)

$$\eta' = \tilde{\omega}_1 - \beta \quad (3)$$

$$\beta' = -\tilde{\omega}_2 + \eta \quad (4)$$

The terms N_1 and N_2 sum aerodynamic, elastic and inertial moments. In this respect, the blade azimuthal coordinate has origin with the blade in the negative direction of the wind axis, and the roll $\bar{p}$ and pitch $\bar{q}$ components of rotor angular velocity are also expressed in wind axes.

The inertial moment components (N_1^i, N_2^i) about the feathering and the flapping axes are, respectively

$$N_1^i = -2I_1\Omega^2(\bar{p}\sin\psi + \bar{q}\cos\psi) \quad (5)$$

$$N_2^i = -2I_2\Omega^2(\bar{p}\cos\psi - \bar{q}\sin\psi) \quad (6)$$

while the elastic ones (N_1^{el}, N_2^{el}), due to the hub and feathering hinge stiffnesses, are

$$N_1^{el} = -K\eta + 2K_T\theta_c \quad (7)$$

$$N_2^{el} = K\beta \quad (8)$$

where K is the hub stiffness, K_T that of the feathering hinges, and θ_c the pitch angle component due to cyclic command. Assuming that the aerodynamic force is applied in the aerodynamic center of the airfoils, aerodynamic moment components N_1^a and N_2^a due, respectively, to paddles and blades are expressed

in closed form as

$$\begin{aligned} N_1^a &= \frac{\gamma_{Fb}}{2}\Omega^2 I_1 \left[\mu^2 J \cos\psi \sin\psi\eta - \tilde{\omega}_1 \right. \\ &\quad \left. + \bar{p}\cos\psi - \bar{q}\sin\psi + \mu J \cos\psi\lambda\right] \qquad (9) \\ N_2^a &= \frac{\gamma_{Bl}}{8}\Omega^2 I_2 \left[-\tilde{\omega}_2 + 2\mu^2 \sin\psi\cos\psi\beta \right. \\ &\quad \left. + (1+2\mu^2\sin^2\psi)\ \theta_c - (\bar{p}\sin\psi + \bar{q}\cos\psi)\right] \\ &\quad - \frac{\gamma_{bl}}{3}\mu\sin\psi\left(\theta_0 + \frac{3}{4}\lambda\right) \qquad (10) \end{aligned}$$

where $J = R_{fb}^2/R^2$ and γ_{bl}, γ_{fb} are, respectively, the Lock numbers of blade and paddle. Note that the paddle surface is limited due also to the high root cut-out, and that the fly-bar is rigidly connected to the hub with the paddle chord parallel to the rotor plane. As usual, the blade pitch angle is the result of the collective θ_0 and cyclic θ_c commands. The latter has two contributions, namely

(i) a primary command $\phi_{SW}\cos\psi - \theta_{SW}\sin\psi$ that corresponds to the longitudinal θ_{SW} and lateral ϕ_{SW} tilts of the swash–plate;
(ii) a secondary command due to the tilt of the hub about the blade feathering axis, that can also be regarded as the fly–bar flapping angle $\theta_{fb} = \eta$.

Therefore, the pitch command (considered as the blade rotation around the feathering axis with respect to the gimbaled yoke) is expressed as

$$\theta = \theta_0 \mp K_H(\phi_{SW}\cos\psi - \theta_{SW}\sin\psi + \eta) \qquad (11)$$

where the gain K_H gives the swash–plate/blade–pitch command ratio. This is something similar to what happens in teetering rotors equipped with a fly–bar, with the major difference that, in the present case, the fly–bar is rigidly connected to the yoke and it directly drives it by means of its flapping motion.

As a result, Eqs. (1)-(4) are rewritten as

$$\begin{aligned} \tilde{\omega}_1' &= -\tilde{\omega}_2 + \frac{\gamma_{fb}}{2}\left[-\tilde{\omega}_1 + \mu^2 J\cos\psi\sin\psi\eta \right. \\ &\quad \left. + (\bar{p}\cos\psi - \bar{q}\sin\psi) + \mu J\cos\psi\lambda\right] \\ &\quad - 2(\bar{p}\sin\psi + \bar{q}\cos\psi) - k_1\eta \\ &\quad - 2k_T K_H(\phi_{SW}\cos\psi - \theta_{SW}\sin\psi \\ &\quad + \eta) \qquad (12) \end{aligned}$$

$$\begin{aligned} \tilde{\omega}_2' &= \tilde{\omega}_1 + \frac{\gamma_{bl}}{8}\left[K_H(1+2\mu^2\sin^2\psi)(\phi_{SW}\cos\psi \right. \\ &\quad - \theta_{SW}\sin\psi + \eta) - \tilde{\omega}_2 \\ &\quad \left. - (\bar{p}\sin\psi + \bar{q}\cos\psi) + 2\mu^2\sin\psi\cos\psi\beta\right] \\ &\quad - \frac{\gamma_{bl}}{3}\mu\sin\psi\left(\theta_0 + \frac{3}{4}\lambda\right) \\ &\quad - 2(\bar{p}\cos\psi - \bar{q}\sin\psi) + k_2\beta \qquad (13) \\ \eta' &= \tilde{\omega}_1 - \beta \qquad (14) \\ \beta' &= -\tilde{\omega}_2 + \eta \qquad (15) \end{aligned}$$

where $k_1 = K/\Omega^2 I_1$, $k_2 = K/\Omega^2 I_2$ and $k_T = K_T/\Omega^2 I_1$. The system can thus be written in concise form as $\dot{\mathbf{x}} = \mathbf{A}(\psi)\boldsymbol{x} + \mathbf{B}(\psi)\mathbf{u}$, the state and control vectors being, respectively, $\mathbf{x} = (\tilde{\omega}_1, \tilde{\omega}_2, \eta, \beta)^T$ and $\mathbf{u} = (\lambda, \theta_{SW}, \phi_{SW}, \bar{p}, \bar{q})^T$. For the sake of simplicity, the inflow parameter λ is regarded as an exogenous input, to be assigned depending on thrust level. The state–matrix of the system (12)–(15) is given by

$$\boldsymbol{A}(\psi) = \begin{bmatrix} -\frac{\gamma_{fb}}{2} & -1 & \frac{\gamma_{fb}}{2}J\mu^2\cos\psi\sin\psi - k_1 - 2k_T K_H & 0 \\ 1 & -\frac{\gamma_{bl}}{8} & \frac{\gamma_{bl}}{8}K_H(1+2\mu^2\sin^2\psi) & \frac{\gamma_{bl}}{4}\mu^2\cos\psi\sin\psi + k_2 \\ 1 & 0 & 0 & -1 \\ 0 & -1 & 1 & 0 \end{bmatrix} \qquad (16)$$

Note that hub tilt can be also described by means of the angles u_1 and u_2 in a non-rotating frame, defined as (Fig. 1)

$$\begin{aligned} u_1 &= -\beta\cos\psi + \eta\sin\psi \qquad (17) \\ u_2 &= -\beta\sin\psi - \eta\cos\psi \qquad (18) \end{aligned}$$

where the angle u_1 is positive when the hub is tilted in the rear direction, while u_2 is positive when it is tilted to the right.

Model validation

As a first step, validation of the simplified model is carried out using a full nonlinear, single–blade simulation model of the gimbaled rotor with rigid blades [7] formulated without small angles assumptions or linearizing techniques in order to analyze the rotor behavior in a variety of motions not limited to small perturbations. Principal features of the general model are

- lift and drag coefficients of blade section are in tabular form for $-180 \le \alpha \le 180$ deg, and for Mach number between zero and 0.8
- aerodynamic loads are computed by numerical integration over the blade span in the framework of blade element approach

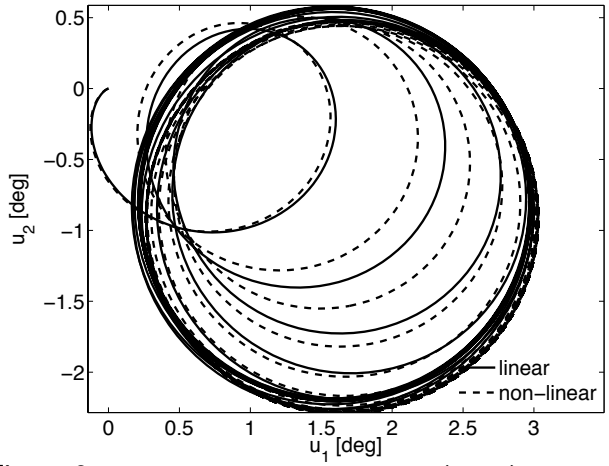

Figure 2: Comparison of the simplified (linear) and general (nonlinear) rotor model responses to a longitudinal cyclic command $\theta_{SW} = 5$ deg; $\mu = 0$, $K = 3,610$ Nm/rad.

- a three–state Pitt-Peters dynamic inflow model [8] is used whereas dynamic stall and unsteady aerodynamics effects are not included
- the rotor is homokinetic, that is, the modules of hub and shaft angular rate vectors are equal

Assuming no coning angle, no twist and no undersling of the blades, Fig. 2 shows a comparison of the hub response (in the u_1-u_2 plane) to a cyclic command $\theta_{SW} = 5^\circ$ in hovering with $K = 3,610$ Nm/rad, as obtained from the simplified and complete models, with the trim value of the rotor thrust $T = 6,400$ N. Rotor data in both cases are shown in Table 1.

It is apparent that the rotor responses obtained from the two models are in good agreement in spite of the large value of the considered cyclic command. In forward flight, the description of the rotor behavior by means of the simplified model becomes less accurate even for relatively small advance ratios, mainly because of the effects of the nonuniform inflow. This is illustrated in Figs. 3 where the response of the tilt angles u_1 and u_2 to a step variation $\mu = 0.05$ of the advance ratio from hovering is reported. The significant differences in the two solutions visible in Fig. 3.a for a rather low advance ratio are due to the non–uniform inflow in the general model, whereas the response is again very similar when a uniform inflow is assumed (Fig. 3.b). If on one side this last result rules out the possibility of adopting the simplified model for a realistic simulation of the full vehicle, on the other one its capability of capturing the fundamental aspects of the motion is demonstrated.

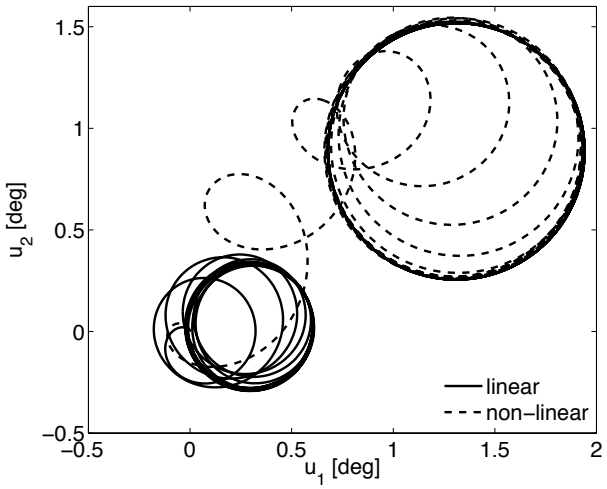

a) general rotor model with 3–states inflow model

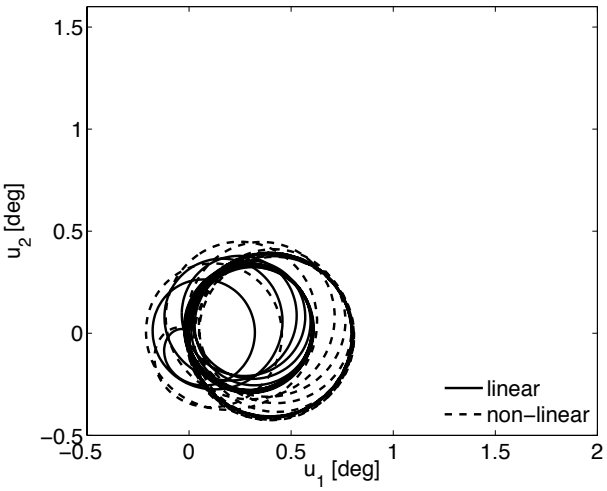

b) general rotor model with uniform inflow

Figure 3: Comparison of the simplified and general rotor model responses to a perturbation of the advance ratio $\mu = 0.05$; $K = 3,610$ Nm/rad.

Table 1: Rotor parameters

rotor angular rate	Ω	53 rad/s
rotor radius	R	3.8 m
blade chord	c_{bl}	0.23 m
fly–bar radius	R_2	1.45 m
fly–bar root cut-out	R_1	1.15 m
paddle chord	c_{fb}	0.25 m
hub stiffness	K	3,610 Nm/rad
feathering hinge stiffness	K_T	150 Nm/rad
primary command ratio	K_H	0.57
blade Lock number	γ_{bl}	4.13
fly–bar Lock number	γ_{fb}	0.53
	J	8.52
	k_1	0.642
	k_2	0.007
	k_T	0.027

Wobbling Motion

As stated previously, one of the most relevant characteristics of the two–bladed gimballed rotor is the onset, in most operating conditions, of a wobbling motion of the rotor hub, which corresponds to a precession motion of the hub axis with respect to the shaft axis. The simplified model [Eqs. (12)–(15)], provides some physical insight into the system that allows for understanding how the wobbling motion is triggered by the periodic loads in the presence of a cyclic pitch command or forward flight condition.

A steady–state condition for the rotor with a constant tilt angle with respect to the shaft axis (that is, without wobbling motion) requires $\tilde{\omega}_1 = \tilde{\omega}_2 = 0$. To this end, the moments N_1 and N_2 need to be constantly zero, which is not true in general, as these terms represent periodic forcing functions.

With reference to Eqs. (1)–(2), assuming a forcing term along the feathering (x_H) axis (Fig. 1) $N_1/(I_1\Omega^2) = A\cos\psi$, the resulting periodic motion at steady–state is $\tilde{\omega}_1' = -\tilde{\omega}_2 = (A/2)\cos\psi$ and $\tilde{\omega}_2' = \tilde{\omega}_1 = (A/2)\sin\psi$. This means that the angular speed components $\tilde{\omega}_1$ and $\tilde{\omega}_2$ continue to oscillate with constant amplitude $A/2$ and phase $\Delta\psi = \pi/2$, thus resulting in a precession motion of the hub axis, namely the wobbling. A similar argument holds for a periodic forcing term around the flapping, $N_2/(I_2\Omega^2) = B\cos\psi$ as, given the system linearity, the perturbed motions can be superimposed.

When considering the effects of cyclic commands in hovering ($\mu = 0$) with zero angular velocity of non–rotating frame ($\bar{p} = \bar{q} = 0$) and zero stiffness of the feathering hinges ($K_T = 0$), all higher–order harmonic terms are zero and Eqs. (12) and (13) become

$$\tilde{\omega}_1' = -\tilde{\omega}_2 - \frac{\gamma_{Fb}}{2}\tilde{\omega}_1 - k_1\eta \quad (19)$$

$$\tilde{\omega}_2' = \tilde{\omega}_1 + \frac{\gamma_{Bl}}{8}\left[K_H(\phi_{SW}\cos\psi - \theta_{SW}\sin\psi + \eta) - \tilde{\omega}_2\right] + k_2\beta \quad (20)$$

With $K = 0$, the steady-state solution is

$$\beta = -\phi_{SW}\sin\psi - \theta_{SW}\cos\psi \quad (21)$$

$$\eta = -\phi_{SW}\cos\psi + \theta_{SW}\sin\psi \quad (22)$$

that gives constant hub tilt angles $u_1 = \theta_{SW}$ and $u_2 = \phi_{SW}$, as obtained by substituting Eqs. (21) and (22) into Eqs. (17) and (18), with the blade tip-path-plane (TPP) parallel to the swash–plate.

Figure 4 shows the system response as function of rotor revolutions in the two considered circumstances following a longitudinal cyclic command. In the ideal case with $K = 0$,the hub angular position achieves a constant value (Fig. 4.a), while in Fig. 4.b the flapping (continuous line) and feathering (dotted line) an-

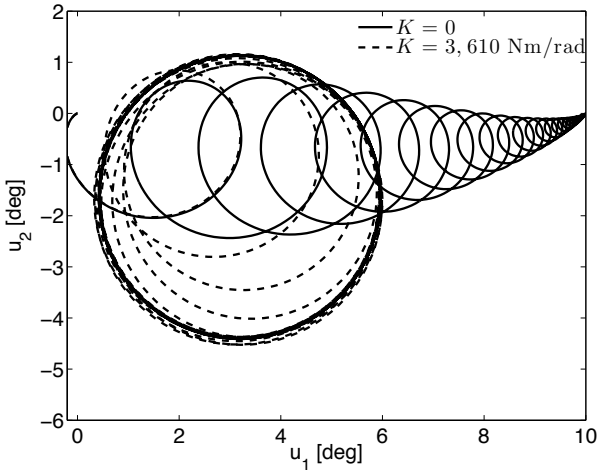

a) hub angular position

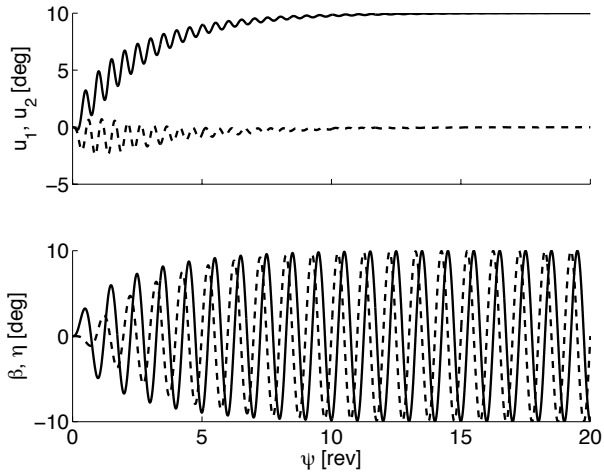

b) hub tilt angles $K = 0$

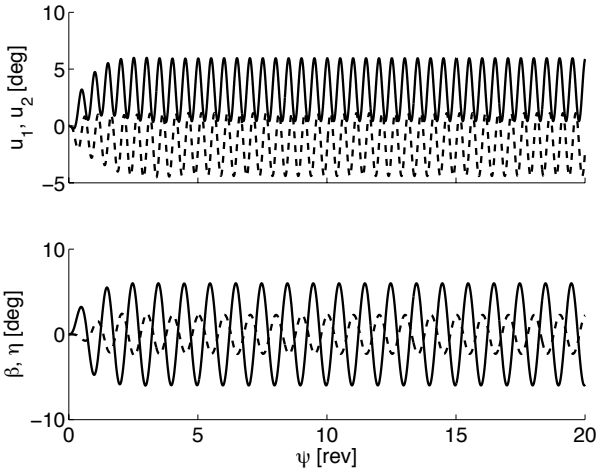

c) hub tilt angles $K = 3,610$ Nm/rad

Figure 4: Response to a longitudinal cyclic command $\theta_{SW} = 10$ deg.

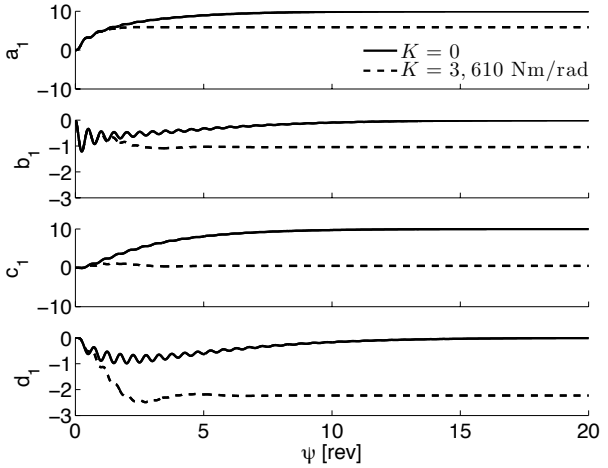

Figure 5: Response to a longitudinal cyclic command $\theta_{SW} = 10$ deg in terms of flapping coefficients.

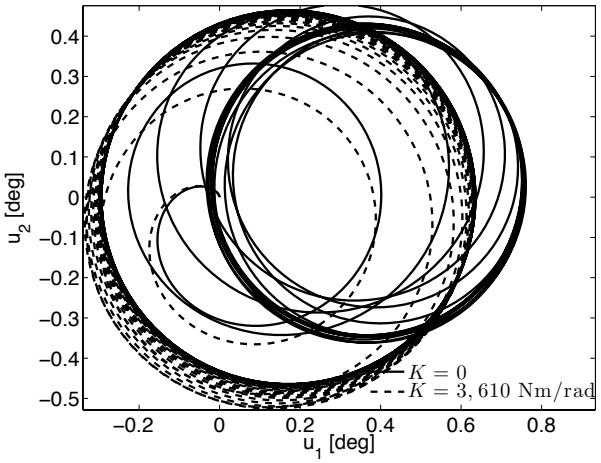

Figure 6: Response to a perturbation of the advance ratio $\mu = 0.05$.

gles show a sinusoidal oscillation in quadrature, and the longitudinal (continuous line) and lateral (dotted line) tilt angles of the TPP, u_1 and u_2, become constant in a time interval corresponding to 15 revs, the time–constant being approximately proportional to the fly–bar inertia I_1.

On the converse, when $K \neq 0$, the TPP angles u_1, u_2 have periodic variations (Fig. 4.c) that prevent the system from achieving a constant equilibrium as the elastic moment about the feathering axis induces a nonzero $\tilde{\omega}_1$ rate that triggers the wobbling motion. In other words, in this case no equilibrium can be established about the feathering axis due to the effect of the periodic elastic moment as, also, the moment of inertia is minimum and the aerodynamic moment of the paddles is small. As far as the equilibrium about the flapping axis is concerned, note that the aerodynamic moment is orders of magnitude higher than the moment due to hub stiffness.

In order to gain some further insight in the wobbling motion characteristics, the feathering and flapping angles can be expressed as

$$\beta = -a_1 \cos\psi - b_1 \sin\psi \quad (23)$$

$$\eta = c_1 \sin\psi - d_1 \cos\psi \quad (24)$$

to introduce the longitudinal a_1, c_1, and lateral b_1, d_1 flapping angles of, respectively, blade and fly–bar TPP's. When Eqs. (23), (24) are substituted into Eqs. (19), (20) written in terms of η and β, application of the harmonic balance method [9] yields a set of differential equations for the TPP flapping degrees of freedom.

Figure 5 shows the responses to a 10 deg longitudinal cyclic command (already illustrated in Fig. 4 considering hub flap and feathering angles) in terms of TPP flapping coefficients. It is worth to observe that after a few rotor revolutions, the orientations of the two planes carved out by blade and paddle tips become constant in spite of the sustained wobbling oscillations in the case with nonzero hub stiffness. As a consequence, the thrust vector direction is constant and, as a further observation, wobbling motion can be interpreted as a 2/rev oscillation of the hub plane between the blade and paddle TPP's, the amplitude of which depends on the relative orientation of the two TPP's. For $K = 0$, when the wobbling motion subsides at steady–state, the TPP's of blades and fly–bar are parallel to the swash–plate ($a_1 = c_1 = \theta_{SW} = 10$ deg, $b_1 = d_1 = \phi_{SW} = 0$). In the case $K \neq 0$, the fly–bar TPP mainly flaps to the left ($c_1 = 0.5$ deg, $d_1 = -2.2$ deg) while the blade TPP is flapping backward ($a_1 = 6$ deg) and to the left ($b_1 = -1$ deg), and the wobbling amplitude is about 6 deg.

When a the response to a step variation of forward speed is considered, Fig. 6 shows that the wobbling motion develops even for $K = 0$ as the moment equilibrium on the feathering axis is now unbalanced by the periodic variation of the aerodynamic moment of the paddles.

As for the effect of the K_H ratio, a lower K_H determines a reduction of the limit cycle amplitude together with a minor effectiveness of the command because the time constant of the rotor response is increased and, in the situation with nonzero K, the hub rotation is smaller for the same cyclic command amplitude.

As shown in Fig. 7, the effect of the feathering hinge stiffness on the evolution and amplitude of the wobbling motion is negligible for the nominal value

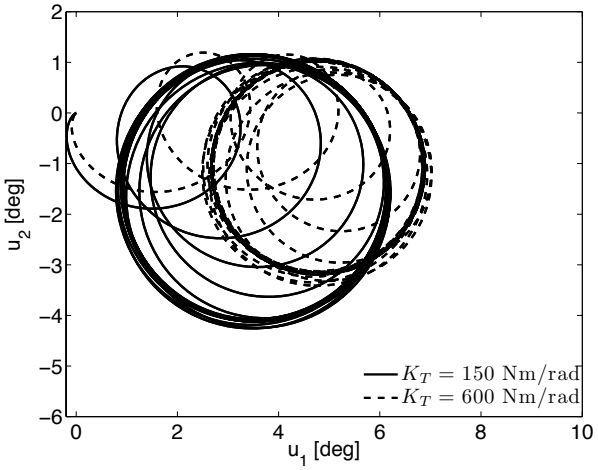

Figure 7: Response to a longitudinal cyclic command $\theta_{SW} = 10$ deg; $K_T \neq 0$.

$K_T = 150$ Nm/rad (the situation with $K_T = 0$ corresponds to the dotted line in Fig. 4.a). Increasing the value of K_T determines a reduction of the limit cycle amplitude together with a major effectiveness of the command at hovering.

As far as the influence of hinge stiffness on wobbling is concerned, it is apparent that the elastic moment along the feathering axis is proportional to θ_c and acts in the sense of reducing the relative orientation of the non-feathering–plane (NFP) and the fly–bar TPP. Therefore, a reduction of the wobbling amplitude due to a restrain action of the pitch hinges can be obtained only in the circumstances, such as hovering, when the angle between NFP and blade TPP is small, while in all the other operating conditions (i.e. advancing flight) the stiffness increases the relative orientation of blade and fly–bar TPP's with the already cited effect of increasing the amplitude of hub oscillatory motion.

Stability Analysis

The periodic terms in the state–matrix $\boldsymbol{A}$ [Eq. (16)] depend on forward speed so that the system achieves a time–invariant form in hovering. In this circumstance Eqs. (19)-(20) can be re–written in terms of flapping and feathering angles. Keeping only the homogeneous terms, the governing equations become

$$\begin{aligned} \beta'' &= -\frac{\gamma_{bl}}{8}\beta' - (1+k_2)\beta - \frac{\gamma_{bl}}{8}(K_H - 1)\eta \\ \eta'' &= -\frac{\gamma_{fb}}{2}\eta' - (1 + k_1 + 2k_T K_H)\eta - \frac{\gamma_{fb}}{2}\beta \end{aligned} \tag{25}$$

Table 2 shows the modal characteristics of this system for $K = 0$ and $K = K_{nom} = 3,610$ Nm/rad,

Table 2: Eigenvalues of the uncoupled system with and without paddles at fly–bar tips.

a) Fly–bar Lock numb. $\gamma_{fb} = 0$		$K = 0$	K_{nom}
Natural frequency ω_n/Ω			
Flapping	$\sqrt{1+k_2}$	1.	1.003
Feathering	$\sqrt{1+k_1'}$	1.	1.282
Damping coefficient ζ			
Flapping	$\frac{\gamma_{bl}}{16}/\sqrt{1+k_2}$	0.261	0.260
Feathering	$\frac{\gamma_{fb}}{4}/\sqrt{1+k_1'}$	0.	0.
b) Fly–bar Lock numb. $\gamma_{fb} = 0.53$		$K = 0$	K_{nom}
Natural frequency ω_n/Ω			
Flapping	$\sqrt{1+k_2}$	1.	1.004
Feathering	$\sqrt{1+k_1'}$	1.	1.281
Damping coefficient ζ			
Flapping	$\frac{\gamma_{bl}}{16}/\sqrt{1+k_2}$	0.255	0.254
Feathering	$\frac{\gamma_{fb}}{4}/\sqrt{1+k_1'}$	0.147	0.115

when small coupling terms are neglected for the sake of simplicity and $k_1' = k_1 + 2k_T K_H$. Two configurations are considered: Case a (reported on the top portion of Tab. 2), when no aerodynamic paddle is present and the resulting fly–bar Lock number is 0; Case b (reported below), when paddles are present and $\gamma_{fb} = 0.53$. For $\gamma_{fb} = 0$ the damping of the feathering motion vanishes, so that a weakly stable system is obtained at hovering. This means that, as already observed in [5] and [6], a regressive motion would be induced on the rotor by the periodic aerodynamic load in forward flight. This characteristics strongly supports the need for the presence of paddles, which thus perform and important stabilizing action for the two–bladed gimbaled rotor, without affecting the characteristics of the flapping mode.

The dynamic analysis of the system supports the interpretation of the effect of hub stiffness on command response illustrated in Figs. 4 and 5. For $K = 0$. flapping and feathering modes are both at resonance so that, as already observed, the blade and fly–bar TTP's are both tilted backward. When the stiffness K takes its nominal value, the feathering frequency is increased and this motion, when represented in terms of TPP position, lags flapping by 77 deg, which turns out in the observed lateral flapping of the fly–bar TPP (Fig. 5). This means that, when the motion is referred to a single angular variable ψ, such that $\psi_{fb} = \psi + \pi/2$, η lags β of 167 deg, which corresponds to what is observed in Fig. 4.

Note also that the sustained wobbling motion at steady–state induces a not negligible variation of the cyclic pitch command, with a 60% reduction of amplitude and a 9 deg phase delay with respect to the situation with $K = 0$. As a consequence, if on one

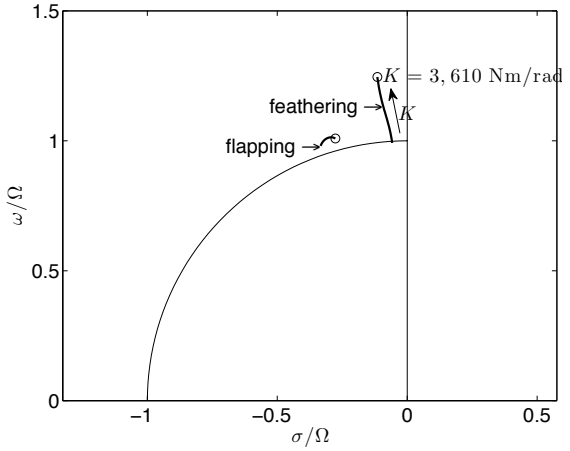

Figure 8: Root locus as a function of K; $\mu = 0$, $k_T = 0$.

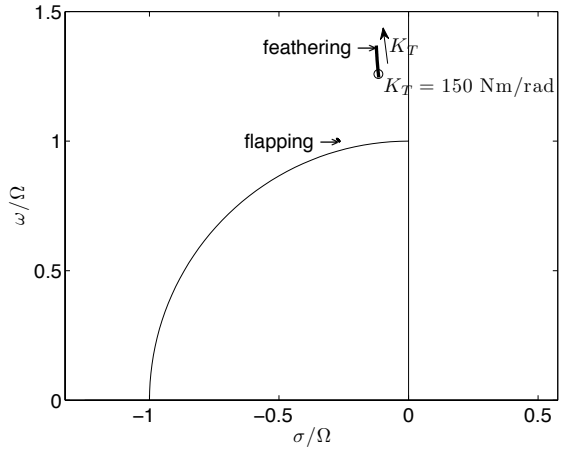

Figure 9: Root locus as a function of K_T; $\mu = 0$, $K = 3,610$ Nm/rad.

side flapping frequency remains close to unity as K is varied (the unit circle corresponding to $\omega_n/\Omega = 1$ is shown in the figures), feathering frequency increases significantly with stiffness, due to the low inertia of the fly–bar, if compared with elastic moments, as demonstrated also by Figure 8. A similar effect on feathering eigenvalues is obtained by increasing the stiffness of the feathering hinges K_T. Figure 9 shows the eigenvalues for K_T varying from 0 to 150 Nm/rad, for the nominal value of K. Again, flapping eigenvalue presents a negligible variation.

Increasing the inertia of the fly–bar leads to the variation of two parameters of the system: the fly–bar Lock number $\gamma_{fb} = 2\rho a_{fb} S_{fb} R_{fb}^3 / I_1$ that decreases the damping of the feathering mode, and the elastic terms, $k_1' = (K + 2K_T K_H)/(\Omega^2 I_1)$, that decreases its natural frequency, resulting in significant variations for the feathering eigenvalue, as shown in Fig. 10. Also in this case only minor variations are observed on the flapping eigenvalue, but I_1 plays a significant role on TPP response to an angular velocity component. In Fig. 11 the response of rotor TPP

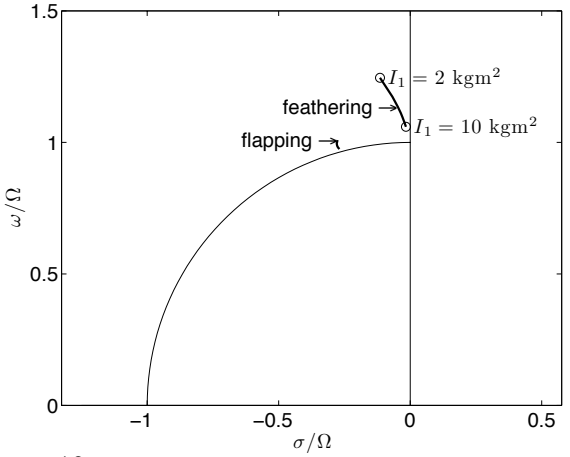

Figure 10: Root locus as a function of I_1; $\mu = 0$, $K = 3,610$ Nm/rad.

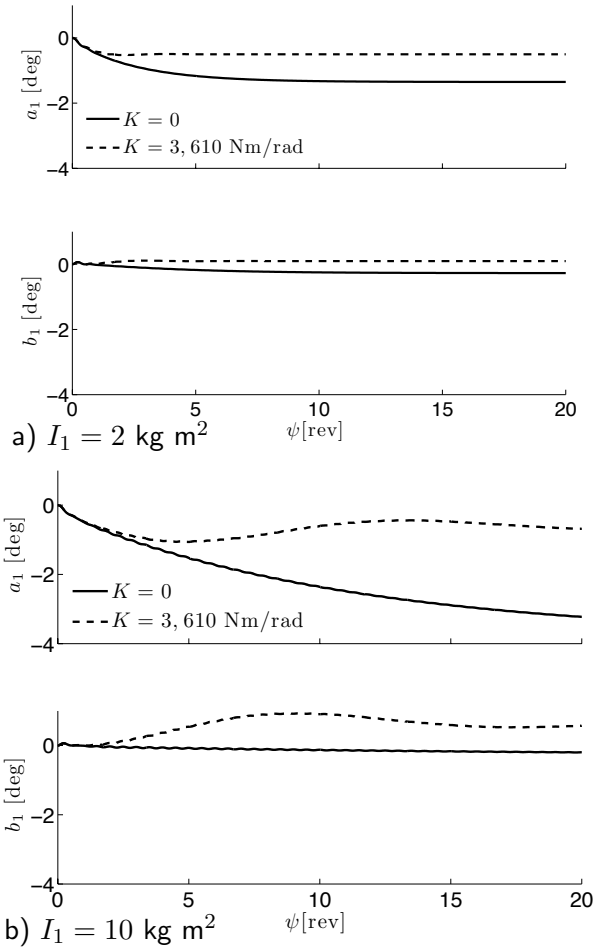

Figure 11: Response in terms of flapping coefficients to a step input on $q = 0.1$ rad/s; $\mu = 0$, $K = 3,610$ Nm/rad.

to a variation on pitch angular velocity is reported, where it is clear how a heavier fly–bar induces a more severe tilt of the TPP, especially for $K = 0$. The effect is reduced by the presence of an elastic gimbal, with a lower response at steady state and less damping, that results in a considerable overshoot.

In forward flight the eigenvalues of the linear, time–

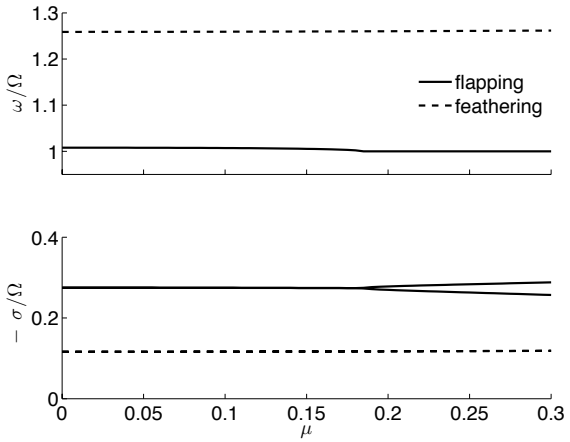

Figure 12: Frequency and damping as a function of μ from Floquet analysis for $K = 3,610$ Nm/rad.

varying system (12)-(15) are determined using Floquet theory [10]. As usual, the state–equation is integrated over one period for each independent initial condition to obtain the Floquet Transition Matrix (FTM). Natural frequencies and damping ratios of the system modes are then obtained by taking the logarithm of the FTM eigenvalues, where use is made of the eigenvalues computed in the hovering condition to identify the origin of the curves. All the roots, reported in Fig. 12, are stable in the considered range of the advance ratio, μ, where the eigenvalues of the feathering mode remain complex, their frequency approximately given by $\omega/\Omega = 1.25$, while those relative to flapping become real for $\mu > 0.18$..

Conclusions

In this paper the dynamic characteristics of a novel two–bladed rotor for a lightweight helicopter have been analyzed using a simplified model in order to interpret the relevant physical mechanisms governing its behavior, and, in particular, the sustained wobbling motion. In this respect, one should note that thrust vector direction is constant in spite of wobbling, as blade TPP does not oscillates at steady–state. Use of a fly–bar with aerodynamics paddles is necessary to damp the feathering motion of the hub, while the classical effect of the stability bar to improve rotorcraft damping derivatives is limited when the hub is restrained by elastomeric springs, adopted in order to retain control power in zero-g flight. Hub stiffness has a relevant effect on the amplitude of wobbling and, in particular, on the steady–state response to commands through the frequency of the feathering motion and the related phase shift. The latter induces a significant reduction of the longitudinal tilt of the blade TPP together with a lateral in response to a longitudinal pitch command.

As a final conclusion, it appears that the considered gimbaled rotor presents favorable stability characteristics and a precession (wobbling) motion the relevance of which is to be carefully assessed using a more detailed model of the rotor where hub undersling, coning hinges and blade elasticity are taken into consideration.

References

[1] Neshat, A.R., "A High Order Simulation Model for the Bell 205 Helicopter", M.Sc. Thesis, Dept. Mechanical and Aerospace Engineering, Carleton University, Ottawa, Ontario, August 1995.

[2] Schrage *et al.*, "Simulation of the Robinson R–22 Helicopter for the Investigation of In–flight Rotor Dynamics", Flight Simulation Laboratory, Georgia Institute of Technology, Atlanta (GA), USA, December 1995.

[3] Johnson, E. N.and Schrage, D., "The Georgia Tech Unmanned Aerial Research Vehicle: GTMax", in AIAA Guidance, Navigation, and Control Conference and Exhibit, (Austin, TX), August 2003.

[4] Chen, R.T.N., "A Simplified Rotor System Mathematical Model for Piloted Flight Dynamics Simulation", NASA TM 78575, Ames Research Center, Moffett Field (CA), USA, May 1979.

[5] Chaplin, H.R., "Some Dynamic Properties of a Rigid Two–Bladed Fully Gimballed Tip–Jet Helicopter Rotor with Circulation Control", TM–16–80/16, David W. Taylor Naval Ship Research and Development Center, Bethesdo (MD), USA, August 1980.

[6] Chaplin, H.R., "Some Dynamic Properties of a Rigid Two–Bladed Fully Gimballed Rotor with Teetering Feedback", TM–16–86/02, David W. Taylor Naval Ship Research and Development Center, Bethesdo (MD), USA, July 1986.

[7] Lucertini, F. "Stability and Flying Qualities of a Light Helicopter", Ph.D. Thesis, Department of Mechanics and Aeronautics, University of Rome "Sapienza", Rome, June 2010.

[8] Peters, D.A., HaQuang, N., "Dynamic inflow for practical applications", Journal of American Helicopter Society, Vol. 33, pp. 64–68, 1988.

[9] Peters, D.A., Ormiston, R.A., "Flapping response characteristics of hingeless rotor blades by a generalized harmonic balance method", NASA TN-D7856, 1975.

[10] Biggers, J.C., "Some approximations to the flapping stability of helicopter rotors", Rotorcraft Dynamics. NASA SP-352, 371 pages, published by NASA, Washington, DC, 1974